Rechargeable Batteries

DOI: 10.1002/anie.201307314

Metal Oxychlorides as Cathode Materials for Chloride Ion Batteries

*Xiangyu Zhao, Zhirong Zhao-Karger, Di Wang, and Maximilian Fichtner**

The ever-increasing energy demands require the development of new rechargeable battery systems, which have high energy density, use abundant material resources, offer high safety, and have environmentally friendly features.[1–5] We previously proposed a new concept of rechargeable chloride ion batteries based on chloride ion transfer.[6] The concept has the advantage of a broad variety of potential electrochemical couples with high theoretical energy density up to values of 2500 $Wh\,L^{-1}$ (Supporting Information, Figure S1), which is close to the theoretical volumetric energy density of the Li/S battery.[7] This new system operated at room temperature includes a metal chloride/metal electrochemical couple and an ionic liquid electrolyte. A key challenge is to suppress the dissolution of cathode materials mainly composed of transition-metal chlorides, which are Lewis acidic and can react with a Lewis base that contains chloride ions, resulting in the formation of soluble complex ions.

Metal oxychlorides (for example, BiOCl, FeOCl, TiOCl, VOCl, $VOCl_2$, and $SnOCl_2$),[8–12] where the metal cations are bound to the strong Lewis basic O^{2-} anion,[13] are more stable than transition-metal chlorides in many organic solvents. This kind of chlorine compound is known to have a layered structure in which adjacent layers are stacked by a van der Waals interaction. For example, BiOCl with a tetragonal structure has a layer in the order of Cl-Bi-O-Bi-Cl (Supporting Information, Figure S2). In BiOCl, the [110] direction is the fastest growth direction during synthesis and the [001] is the slowest owing to the weak *c*-axis bonding,[14] facilitating the formation of a flake-like morphology. Song et al. reported that BiOCl could lose chlorine and decompose into BiO and Cl_2 by heat treatment in N_2 flow.[15] Moreover, metal oxychloride/metal systems could also show a large Gibbs free energy change yielding a high electromotoric force (EMF) during the chloride ion transfer. For instance, the $VOCl_2$/Li electrochemical couple possesses a high EMF of 2.78 V and a theoretical energy density of 984.2 $Wh\,g^{-1}$ (Supporting Information, Figure S1). Therefore, it should in principle be possible to use this kind of chlorine compound as cathode material for chloride ion batteries. The overall reaction for this battery could be expressed as:

$$m\,M_cOCl_n + n\,M_a \leftrightarrow m\,M_cO + n\,M_aCl_m \quad (1)$$

where M_c is the metal element in the cathode, M_a is the metal used in the anode, and *m* or *n* is the number of chloride ions.

Herein, we report a new type of chlorine compound, metal oxychloride, as potential cathode material for chloride ion batteries. The electrochemical performance and the reaction mechanisms of the BiOCl and FeOCl cathode were investigated. Both cathodes showed reversible reactions, including a major conversion reaction and a minor intercalation process, by chloride ion transfer during cycling. The FeOCl cathode possessed a stable discharge capacity of 60 $mA\,h\,g^{-1}$ after several initial cycles.

Figure 1 shows the discharge and charge curves and CV patterns of the BiOCl/Li system using an electrolyte of 0.5 M

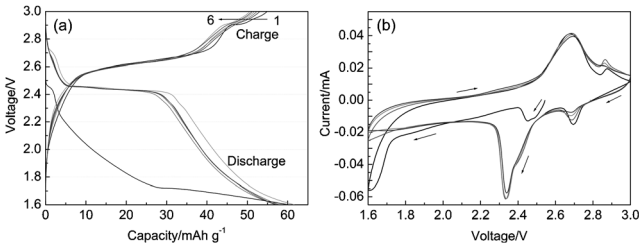

Figure 1. a) Discharge and charge curves (1st to 6th cycles, 5 $mA\,g^{-1}$) and b) CV patterns (1st to 4th cycles, 50 $\mu V\,s^{-1}$) of the BiOCl/Li system using an electrolyte of 0.5 M $N_{116(14)}Cl$ in $N_{1114}TFSI$ at 298 K.

$N_{116(14)}Cl$ in $N_{1114}TFSI$, which has an ionic conductivity of 0.73 $mS\,cm^{-1}$ at 298 K. The BiOCl cathode shows a discharge capacity of 60 $mA\,h\,g^{-1}$, which is 59% of the theoretical capacity (103 $mA\,h\,g^{-1}$), and a low discharge plateau at the first cycle, as shown in Figure 1a. This electrochemical polarization may be caused by slow charge transfer and chloride ion diffusion, which is ascribed to the relatively large particle size of as-prepared BiOCl material as shown in SEM image (Supporting Information, Figure S3). It is likely that the conversion reaction refines the particle size and leads to the formation of large fresh and active surface, an effect which has been observed for a number of conversion materials. The activation process also exists at the anode side. Therefore, the voltage plateau of the BiOCl/Li system in the second discharge increases to 2.4 V. The corresponding voltage plateau for the subsequent charge is at 2.65 V. A narrow voltage hysteresis between discharge and charge was observed for the BiOCl/Li system. The CV curve of the

[*] Dr. X. Y. Zhao, Dr. Z. Zhao-Karger, Dr. D. Wang, Prof. Dr. M. Fichtner
Institute of Nanotechnology
Karlsruhe Institute of Technology (KIT)
Postfach 3640, 76021 Karlsruhe (Germany)
E-mail: m.fichtner@kit.edu
Dr. X. Y. Zhao
College of Materials Science and Engineering
Nanjing University of Technology (China)
Dr. D. Wang
Karlsruhe Nano Micro Facility, KIT (Germany)
Prof. Dr. M. Fichtner
Helmholtz Institute Ulm (HIU) for Electrochemical Energy Storage
89081 Ulm (Germany)

Supporting information for this article is available on the WWW under http://dx.doi.org/10.1002/anie.201307314.

BiOCl/Li system (Figure 1b) exhibits two distinct pairs of cathodic and anodic peaks under the potential window of 1.6–3.0 V. The first reduction peak appears at 2.69 V and the corresponding oxidation peak is observed at 2.89 V. This small redox couple reflects the stages of initial discharge and final charge after the first cycle in Figure 1a. Another large redox couple at low potential corresponds to the main reactions in the cycling, dominating the capacity of the BiOCl/Li system. An electrochemical test using an electrolyte of 0.5 M $PP_{14}Cl$ in $PP_{14}TFSI$ with an ionic conductivity of 0.61 mS cm^{-1} at 298 K was also performed (Supporting Information, Figure S4). The BiOCl/Li system shows similar electrochemical characteristics in this electrolyte.

Figure 2a shows the XRD patterns of the BiOCl cathode at the first cycle using the electrolyte of 0.5 M $N_{116(14)}Cl$ in

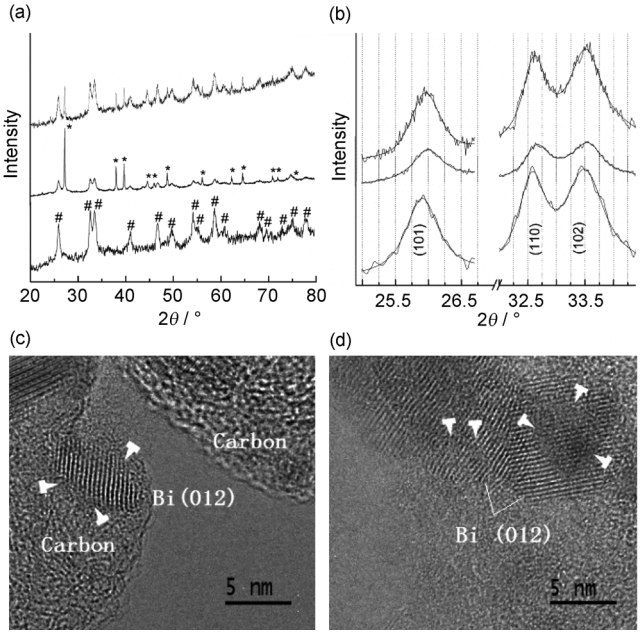

Figure 2. a,b) XRD patterns of the BiOCl cathode at the first cycle using the electrolyte of 0.5 M $N_{116(14)}Cl$ in $N_{1114}TFSI$ at 298 K. Bottom curves: As-prepared BiOCL, middle: first discharge; top: first charge. ⋆ Bi (PDF card no. 5-519); # BiOCl (PDF card no. 6-249). c,d) HRTEM images of the BiOCl cathode after discharge.

$N_{1114}TFSI$. Bi metal is formed while a part of the oxychloride still exists after discharge. In the charged electrode, the intensity of Bi metal peaks is drastically decreased and the BiOCl phase is recovered by the reversible oxidation reaction shown in the CV pattern (Figure 1b). The SAED result (Supporting Information, Figure S5) confirms this phase transformation. Note that there is a peak shift of oxychloride phase during discharge and charge (Figure 2b). The peaks corresponding to the (101), (110), and (102) lattice planes shift to higher angles with about 0.1°, 0.1°, and 0.05° after discharge, respectively. This indicates that a lattice contraction of oxychloride occurs during discharge, that is, when part of Cl is stripped off the BiOCl. The lattice was almost recovered, as is evident from the return of the diffraction peaks after the subsequent charge. The process that the oxychloride keeps its crystal structure without phase transformation could be ascribed to an intercalation reaction of chloride ion ($BiOCl \rightarrow BiOCl_{1-x}$, $x > 0$), which leads to the formation of the redox couple at high voltage in the CV pattern (Figure 1b). The major electrical charge at low voltage could be attributed to the conversion reaction. During the discharge, the BiOCl loses the chloride ion and should transform to BiO. Nevertheless, BiO is unstable and may decompose to Bi metal and Bi_2O_3, which has a monoclinic structure (PDF card no. 14-699) at room temperature. However, the pattern of Bi_2O_3 was not detected by XRD and SAED (Supporting Information, Figure S5). Figure 2c,d shows the HRTEM images of the BiOCl sample after discharge. The lattice fringe is assigned to the (012) lattice plane of Bi metal. Moreover, some amorphous phases around and/or blending with the Bi phase are observed, as shown in the area marked with white arrows. This suggests that the Bi_2O_3 exists in amorphous form.

STEM and the corresponding EELS were carried out to get further insight in the reaction mechanism of the BiOCl cathode. Ball milling leads to cracking of the as-received BiOCl flakes (Supporting Information, Figure S2) and results in the formation of a needle-like morphology in the as-prepared BiOCl sample, as shown in the STEM image in Figure 3a. The corresponding Cl L-edge EELS pattern shows a peak appearing at 200 eV. The reduction of BiOCl in the discharge stage results in the formation of Bi metal and

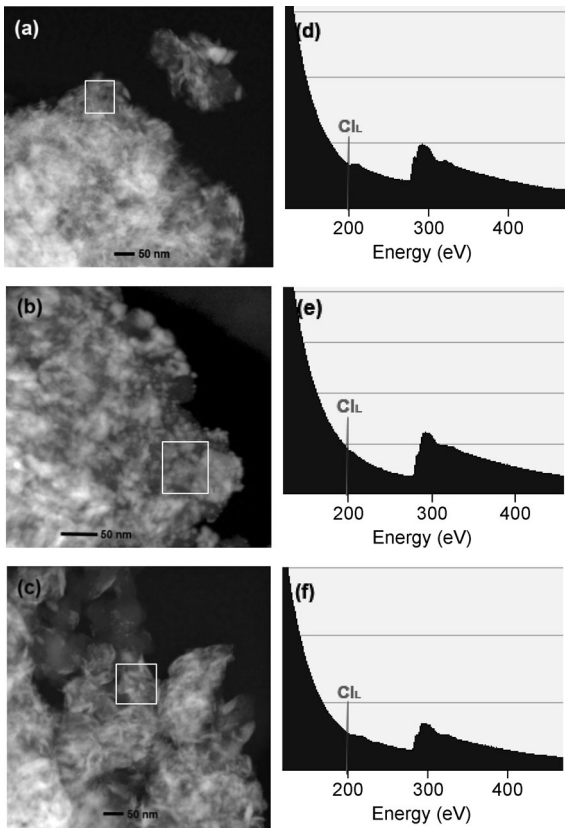

Figure 3. STEM images (scale bars: 50 nm) and the corresponding Cl L-edge EELS patterns of the BiOCl cathode at the first cycle: a,d) as-prepared BiOCl; b,e) discharge; and c,f) charge.

amorphous Bi_2O_3, inducing a considerable change in the morphology from needle-like to granular. The loss of chloride ion in this stage was also confirmed by the EELS result, as shown in Figure 3e. In the charged electrode, the same morphology as that of the as-prepared BiOCl is observed. Moreover, the chloride ion moves back to the cathode side, as shown in Figure 3f. The polyphase reaction among Bi metal, amorphous Bi_2O_3, and chloride ion contributes to the recovery of BiOCl phase after charge. STEM and EELS results further and more directly prove the reversible reactions mentioned above.

A further investigation on metal oxychloride cathodes was performed by using the orthorhombic layered FeOCl material. The structure and composition of the obtained product prepared by the solid-gas reaction was assigned to FeOCl phase, as confirmed by the XRD and EDX results (Supporting Information, Figure S6). This product shows a uniform morphology (Figure S6b) and a strong diffraction peak at (010) plane. After ball milling, the FeOCl material maintained its crystal structure. However, the peak intensity of (010) plane was drastically reduced by the fracture process caused by ball milling owing to the weak *b*-axis bonding.

Figure 4a shows the discharge and charge curves of the FeOCl/Li system using an electrolyte of 0.5 M $PP_{14}Cl$ in

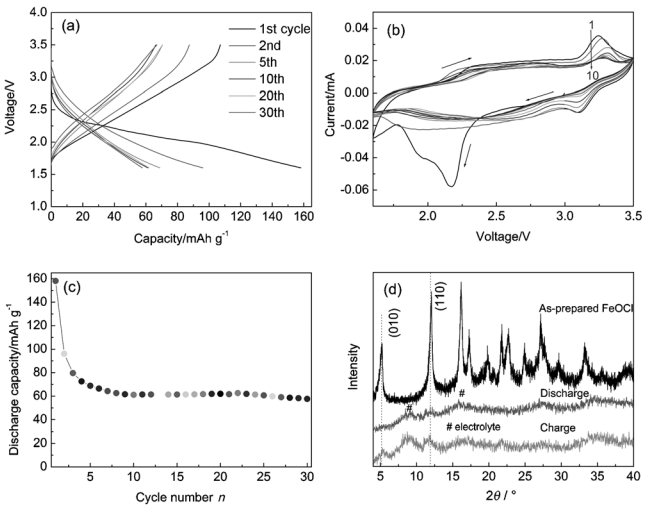

Figure 4. a) Discharge and charge curves (10 mA g^{-1}), b) CV patterns (1st to 10th cycles, 60 μV s^{-1}), c) cycling performance of the FeOCl/Li system, and d) XRD patterns of the FeOCl electrode using the electrolyte of 0.5 M $PP_{14}Cl$ in $PP_{14}TFSI$ at 298 K.

$PP_{14}TFSI$ at 298 K. This system presents similar sloping discharge and charge profiles during different cycles. The middle voltage values for the discharge and charge are 2.1 and 2.6 V, respectively. The FeOCl cathode shows a discharge capacity of 158 mA h g^{-1}, which is 63% of the theoretical capacity (250 mA h g^{-1}). Moreover, a charge capacity of 107 mA h g^{-1}, that is, 68% of the discharge capacity, could be recovered in the first cycle. The discharge capacity decreases in the initial several cycles and then is stabilized at around 60 mA h g^{-1} (Figure 4c). The capacity decay in initial cycles may be ascribed to the interruption of electrical contact between partial active material and carbon black during cycling. Note that a large volume contraction (−58.6%) or expansion (141.7%) can occur during the phase transformation between FeOCl and FeO. These values are much larger than −24.7% and 32.7% for the BiOCl electrode during chloride ion transfer, an appropriate microstructure of the electrode material will therefore be essential if stable cycling behavior shall be accomplished. The CV patterns of the FeOCl/Li system (Figure 4b) obtained under the potential window of 1.6–3.5 V also exhibit electrical charge decay in the initial cycles. This is consistent with the result of the discharge and charge testing. Similar to the BiOCl/Li system, the FeOCl/Li system also shows two redox couples in the CV patterns. A small distinct redox couple at high voltage has a reduction peak at 3.1 V and the corresponding oxidation peak at 3.27 V. Another large redox couple at low potential shows a broad reduction region at 2.9–1.8 V and the corresponding oxidation region at 2.0–3.0 V, which is in accordance with the sloping discharge and charge profiles in Figure 4a. These two electrochemical steps may be attributed to a major conversion reaction and a minor intercalation process, as described in the BiOCl/Li system.

Figure 4d shows the XRD patterns of the FeOCl electrode at the first cycle. The diffraction peaks corresponding to FeOCl phase vanish after discharge. However, no diffraction peaks corresponding to FeO are observed, which may be explained by the formation of amorphous and/or nanosized particles. The broad diffraction peaks in the discharged and charged samples are assigned to the reflection of electrolyte of 0.5 M $PP_{14}Cl$ in $PP_{14}TFSI$. In the charged electrode, the diffraction peaks corresponding to (010) and (110) planes of FeOCl phase appear, indicating the reversible reaction by the recharge or oxidation process. STEM and the corresponding EDX (Supporting Information, Figure S7) were performed for the FeOCl electrode before and after cycling. Similar to the BiOCl electrode, the FeOCl electrode also showed a distinct morphology change during cycling, from needle-like to ultrafine granular after discharge and then back to needle-like after charge. The EDX result demonstrates the loss of chloride ion during discharge, resulting in the formation of iron oxide. Moreover, the chloride ion moves back to the cathode after charge. This is consistent with the XRD result in Figure 4d. HRTEM images and the corresponding fast Fourier transform (FFT) pattern of the FeOCl electrode after discharge in Figure 5 were performed to get a further insight in the structure of the discharged sample, which has an ultrafine particle/grain size of 2–3 nm (Figure 5a). The digital diffractogram (Figure 5b) in the FFT can be indexed to cubic Fe_3O_4 (PDF card no. 2-1035) structure. The formation of Fe_3O_4 could be attributed to the oxidation of FeO during the TEM test, which has an ultrafine size and is extremely sensitive.

In summary, we have investigated bismuth oxychloride and iron oxychloride as cathode materials for the chloride ion battery. The BiOCl cathode shows a reversible capacity of about 60% of the theoretical capacity, which is mainly derived from the conversion reaction. An intercalation reaction during cycling is also observed. In the discharge stage, the BiOCl loses the chloride ion and transforms to Bi

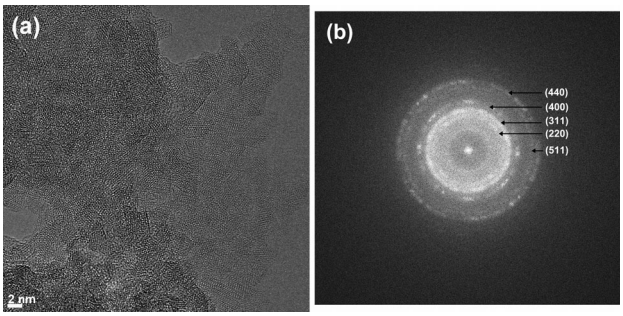

Figure 5. a) HRTEM image (scale bar: 2 nm) and (b) the corresponding FFT pattern of the FeOCl electrode after discharge using the electrolyte of 0.5 M $PP_{14}Cl$ in $PP_{14}TFSI$ at 298 K.

metal and amorphous Bi_2O_3, with a considerable morphology change from needle-like to granular. The return of chloride ion during charge results in the recovery of BiOCl phase at the cathode side. The FeOCl cathode also shows reversible reactions based on the chloride shuttle. It possesses a discharge capacity of 158 $mA\,h\,g^{-1}$at the first cycle and a stable discharge capacity of 60 $mA\,h\,g^{-1}$ in 30 cycles. These results suggest that metal oxychloride is a promising cathode material for chloride ion batteries.

Experimental Section

Bismuth oxychloride (BiOCl, 98%, Alfa Aesar) was dried at 90°C for 24 h under vacuum. The BiOCl cathode material was prepared by ball-milling BiOCl and 25 mass% carbon black using a 125 mL tungsten carbide vial with tungsten carbide balls (10 mm in diameter) under an argon atmosphere. The ball to powder ratio was 50:1. The milling was performed in a planetary mill with a rotation speed of 350 rpm and the milling time was 25 h. FeOCl was prepared by a solid–gas reaction.[8] A mixture of α-Fe_2O_3 (99.99%, Alfa Aesar) and anhydrous $FeCl_3$ (99.7%, ChemPur) with a molar ratio of 3:4 was loaded in an evacuated and sealed quartz tube, and then heat treated at 633 K for six days with a heating and cooling rate of 1 $K\,min^{-1}$. Afterwards, the tube was opened and the purple powders were washed with acetone to remove the residue iron chloride in glove box, followed by an overnight drying at 358 K under vacuum. This product was ball milled for 20 min at 200 rpm using silicon nitride vial (80 mL) and balls (10 mm in diameter), and then mixed with 25 mass% carbon black for another 20 min of ball milling to form a FeOCl/carbon black composite as the cathode material. The anhydrous ionic liquids of butyltrimethylammonium bis(trifluoromethylsulfonyl)imide ($N_{1114}TFSI$, 99%, Sigma–Aldrich), benzyldimethyltetradecylammonium chloride ($N_{116(14)}Cl$, 99%, Sigma–Aldrich), 1-butyl-1-methylpiperidinium bis(trifluoromethylsulfonyl)imide ($PP_{14}TFSI$, 99%, IoLiTech), and 1-butyl-1-methylpiperidinium chloride ($PP_{14}Cl$, 99%, IoLiTech) were all dried at 358 K for 72 h under vacuum. The BiOCl and FeOCl samples were found to be stable in the electrolyte by 2 months of immersion testing.

X-ray powder diffraction was performed using a Philips X'PERT diffractometer with Cu-Kα or Mo-Kα radiation. Transmission electron microscopy was performed on a Titan 80-300 aberration corrected electron microscope, operated at an accelerating voltage of 300 kV. Scanning transmission electron microscopy (STEM) images were acquired by a high-angle annular dark field (HAADF) detector (Fischione Instruments). Electron energy loss spectroscopy (EELS) and energy-dispersive X-ray spectroscopy (EDX) patterns were obtained in STEM mode. The samples for TEM test were thoroughly washed with acetone (99.8%) or methanol (99.9%) in a Schlenk tube under argon atmosphere, to remove the electrolyte.

Electrochemical measurements were conducted using two-electrode Swagelok-type cells with lithium metal as anode. The cathode electrodes were fabricated by mixing as-synthesized material, PVDF, and carbon black in the mass ratio of 80:10:10. *N*-Methyl-2-pyrrolidinone (NMP) was used as the solvent for PVDF to get homogeneous slurry, which was spread on a stainless steel (SS) foil and dried on hot plate at 393 K for 20 h. A mixture of 0.5 M $N_{116(14)}Cl$ in $N_{1114}TFSI$ or 0.5 M $PP_{14}Cl$ in $PP_{14}TFSI$ was used as electrolyte. Glass fiber (GF/D; Whatman) was used as separator. Discharge and charge tests were carried out galvanostatically at 5 or 10 $mA\,g^{-1}$ over a voltage range between 3.0 or 3.5 and 1.6 V by using Arbin BT2000 multi-channel battery testing system at 298 K. The specific capacities were calculated according to the corresponding active material of the cathode electrode. Cyclic voltammetry (CV, 1.6 to 3.0 or 3.5 V, 50 or 60 $\mu V\,s^{-1}$) was performed using an AUTOLAB electrochemical workstation.

Received: August 20, 2013
Published online: November 7, 2013

Keywords: chloride ions · electrochemistry · ionic-liquid electrolytes · metal oxychlorides · rechargeable batteries

[1] B. Goodenough, K. S. Park, *J. Am. Chem. Soc.* **2013**, *135*, 1167–1176.
[2] Y. Yang, G. Y. Zheng, S. Misra, J. Nelson, M. F. Toney, Y. Cui, *J. Am. Chem. Soc.* **2012**, *134*, 15387–15394.
[3] J. Muldoon, C. B. Bucur, A. G. Oliver, T. Sugimoto, M. Matsui, H. S. Kim, G. D. Allred, J. Zajicek, Y. Kotani, *Energy Environ. Sci.* **2012**, *5*, 5941–5950.
[4] N. Yabuuchi, M. Kajiyama, J. Iwatate, H. Nishikawa, S. Hitomi, R. Okuyama, R. Usui, Y. Yamada, S. Omaba, *Nat. Mater.* **2012**, *11*, 512–517.
[5] R. Mohtadi, M. Matsui, T. S. Arthur, S. J. Hwang, *Angew. Chem.* **2012**, *124*, 9918–9921; *Angew. Chem. Int. Ed.* **2012**, *51*, 9780–9783.
[6] X. Y. Zhao, S. Ren, M. Bruns, M. Fichtner, *J. Power Sources* **2014**, *245*, 706–711.
[7] P. G. Bruce, S. A. Freunberger, L. J. Hardwick, J. M. Tarascon, *Nat. Mater.* **2012**, *11*, 19–29.
[8] L. Armelao, G. Bottaro, C. Maccato, E. Tondello, *Dalton Trans.* **2012**, *41*, 5480–5485.
[9] M. D. Lind, *Acta Crystallogr. Sect. B* **1970**, *26*, 1058–1062.
[10] M. Shaz, S. V. Smaalen, L. Palatinus, M. Hoinkis, M. Klemm, S. Horn, R. Claessen, *Phys. Rev. B* **2005**, *71*, 100405.
[11] V. H. Oppermann, *Z. Anorg. Allg. Chem.* **1967**, *351*, 113–124.
[12] K. Dehnicke, *Z. Anorg. Allg. Chem.* **1961**, *308*, 72–78.
[13] I. D. Brown, *Acta Crystallogr. Sect. B* **1988**, *44*, 545–553.
[14] H. L. Peng, C. K. Chan, S. Meister, X. F. Zhang, Y. Cui, *Chem. Mater.* **2009**, *21*, 247–252.
[15] J. M. Song, C. J. Mao, H. L. Niu, Y. H. Shen, S. Y. Zhang, *CrystEngComm* **2010**, *12*, 3875–3881.

